Lasers in Manufacturing Conference 2015

Femtosecond laser ablation in liquids of iron-based nanoparticles

A. Kanitz, J. S. Hoppius, M. Chakif, E. L. Gurevich, A. Ostendorf

Applied Laser Technologies, Ruhr-University Bochum, Universitätsstr.150, 44801 Bochum, Germany

Abstract

Nanoparticles are intensively investigated in several fields of research due to their wide range of properties and potential applications. Especially magnetic nanoparticles are of great interest in the field of magnetic fluids, catalysis, biotechnology/biomedicine, magnetic resonance imaging, data storage, and environmental remediation.
Pulsed laser ablation in liquids (PLAL) is a simple method for the rapid production of colloidal nanoparticles. The technique requires a suitable laser source, the desired target material and a liquid. One further advantage of the PLAL produced particles is the ligand-free surface which makes them chemically more active than chemical synthesized ones [1,2].
Here, we present a study on the generation of magnetic iron-based nanoparticles generated by high power femtosecond PLAL with peak powers up to 10^{10} watts. We discuss the influence of the used liquid and applied laser parameters on the generated nanoparticle properties. These properties, size distribution, shape and composition are investigated by several methods, e.g. TEM, EDX, dynamic light scattering, and Raman spectroscopy.

Keywords: femtosecond laser, laser ablation, magnetic nanoparticles

1. Introduction

Magnetic iron-based nanoparticles are of great interest in various fields. Reaching from magnetic fluids [1], catalysis [2], biotechnology/biomedicine [3], magnetic resonance imaging [4], data storage [5] and environmental remediation [6]. Lately, they have also been used in laser based technologies like two-photon polymerization and holographic optical tweezers to exploit their magnetic properties for the control of micro-fluidic devices [7] and micro-actuators [8].

As a laser-based nanoparticle production method, pulsed laser ablation in liquids (PLAL) has been established in recent years for a simple production of colloidal nanoparticles [9, 10]. A laser pulse evaporates solid material into a liquid environment where nanoparticles condensate from supersaturated metal vapor. With this technique, it is possible to obtain nanoparticles which are hardly accessible by chemical production methods. As further advantage, the particles are ligand-free which makes them chemically more active than chemically synthesized nanoparticles [11].

PLAL of iron and iron-based materials has been studied by several groups to deepen the understanding of the process and to tailor the properties of the magnetic nanoparticles. Amendola et al. conducted research on the creation of iron-based nanoparticles by nanosecond-PLAL in different liquids [12, 13]. Further Franzel et al. [14] investigated PLAL of iron by 750 ps pulses yielding the same results as different other authors using nanosecond pulses for producing nanoparticles from iron in liquid environments [15–18]. To the knowledge of the authors, this is the first study on femtosecond-PLAL of iron in liquid environments.

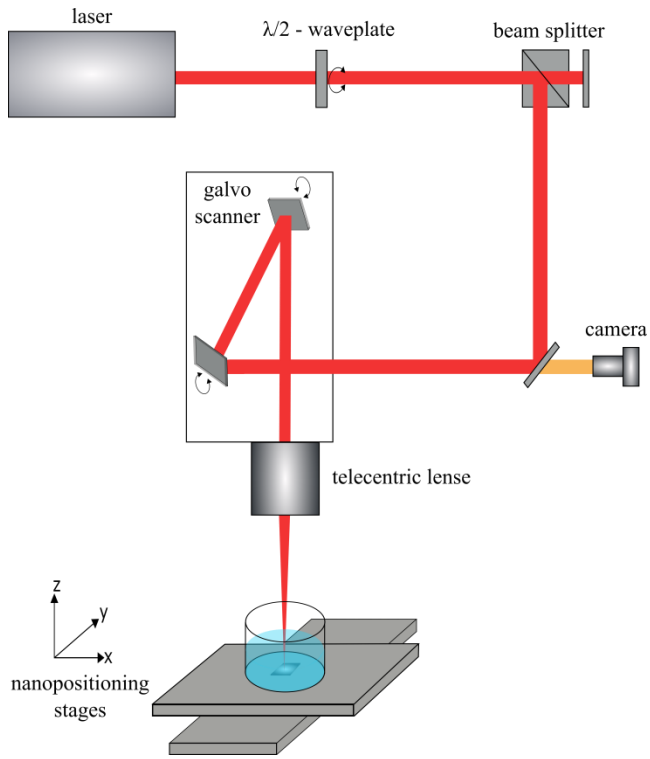

Figure 1: Scheme of the experimental setup for fs-PLAL in a batch chamber.

The aim of this work is to obtain knowledge about the production process, the resulting particle composition and size distribution for further tailoring of the magnetic properties of the nanoparticles. Femtosecond pulsed laser ablation is different to nanosecond-PLAL. As a consequence of the fast energy delivery and decoupling of laser beam impact and plasma generation, the plasma exhibits higher temperatures and faster cooling rates.

2. Experimental

2.1. Synthesis and ablation strategy

The generation of nanoparticles has been carried out by using a Spectra-Physics SpitFire Ace System as laser source: A 5 W system with a minimal pulse duration of 35 fs and repetition rate of 5 kHz resulting in a maximal pulse energy of 1 mJ per pulse at a central wavelength of 800 nm. The experimental setup is shown in Figure 1. The power of the laser beam is controlled by a λ/2-waveplate in combination with a polarizing beam splitter. Further, the beam is guided through a galvo-scanner onto the target. The target and scanner are connected to an x-y-z nanopositioning system that allows precise control of the laser processing position and speed on the target.

The presented measurements have been carried out at an optimal fluence [19, 20] of 0.3 J/cm² with respect to the optical path within the liquid. Furthermore, the scanning velocity was adapted for each used pulse energy to have sufficiently separated pulses for an efficient bypassing [21]. Therefore the influence of cavitation bubbles, heat accumulation [22] and nanoparticle post processing [23, 24] on the production process was limited.

In the study presented, we used two different liquids, Acetone and HPLC-Water, in order to study the effect of an organic and inorganic liquid on the particle composition. The used target was an Fe-target (Goodfellow GmbH, purity 99,5%).

2.2. Characterization

To obtain information on the particle size, morphology and composition, transmission electron microscopy (TEM) measurements were carried out using an FEI Tecnai F20 system operating at 200 kV. For the TEM measurements, some drops of the nanoparticle solution have been evaporated on a copper grid covered with a thin amorphous carbon film.

For the hydrodynamic diameter determination of the nanoparticles, dynamic light scattering (DLS) measurements were carried out by a MicroTrek Nanoflex 180° system.

All measurements have been carried out at room temperature.

3. Results

3.1. Optimal ablation efficiency in acetone and water

In the study presented, the dependency of the particle size distribution and particle composition on the pulse energy at optimal ablation efficiency was investigated. The implications of using different fluences shows that working at optimal efficiency yields a maximum of ablated volume as well as less heat accumulation at the target surface. A detailed theoretical description is given elsewhere [19, 20], but from these studies arises that the optimal working point is found at a fluence of $F = e^2 * F_{th}$ for a Gaussian beam. Beside the advantage of working at optimal efficiency, other benefits by using the optimal working point occur. Firstly, one can compare the influence of the nanoparticle properties generated by different laser systems with different maximal pulse energies at maximum ablation rate. Secondly, the penetration depth of the laser pulse is almost constant while the spot sizes changes. Thus, the influence of the spot size can be investigated.

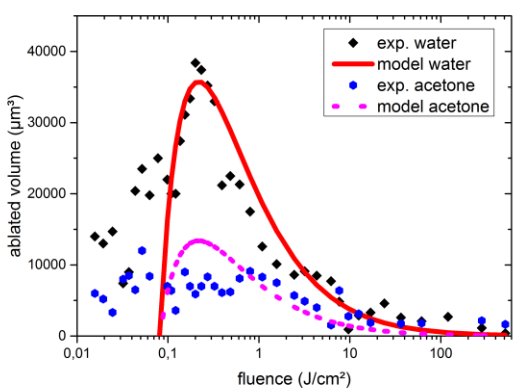

Figure 2: Ablated volume for 20 single shots for different fluences in water and acetone fitted with model curves.

The optimal ablation fluence was determined and validated experimentally to further use this data to evaluate the dependency of size distribution and particle composition on pulse energy.

For the determination of the optimal working point, a polished target was placed in a batch chamber. After ablating 20 spots at a specified fluence, the ablated volume was determined by white-light interferometry (compare Figure 2). As mentioned before, the theoretical efficiency has been investigated by Neuenschwandner et al. for laser ablation in air [19] and by Intartaglia et al. in deionized water [20]. From these investigations, the experimental results could be fitted with the formula:

$$V_{20}(F) = \alpha(1-R)\frac{E_0}{F}\ln^2\left(\frac{F}{F_{th}}\right)$$

V_{20} is the ablated volume after 20 shots on the same position. Due to complex physicochemical processes in PLAL which reduce the ablated volume, the fitting parameter α was introduced. R is the reflectivity, E_0 is the pulse energy, F is the fluence, which is referred to the fluence calculated with respect to the linear optical path which may differ from the real fluence due to non-linear beam propagation, e.g. self-focusing and filamentation.

Figure 2 shows the maximum ablation in water and acetone at a fluence of 0.2 to 0.3 J/cm² which is a realistic value.

The difference of ablated volume between water and acetone may occur due to the complex effects involved in laser ablation in liquid environments such as plasma-confinement by the liquid which is dependent on the liquid properties such as compressibility, viscosity and density at different temperatures.

3.2. Influence of pulse energy at optimal ablation efficiency on nanoparticle size distribution and particle composition in acetone

The influence of the pulse energy at optimal efficiency on particle size distribution in acetone was investigated for pulse energies ranging from 10 µJ to 800 µJ. For the sake of simplicity and visibility, two exemplary size distributions, at 10 µJ (black) and 800 µJ (red) are shown (compare Figure 3). These curves show the hydrodynamic size distribution measured by dynamic light scattering. Typical for PLAL generated size distributions, both curves are in agreement with a lognormal size distribution. They possess a particle number size maximum at 99 and 76 nm and with a corresponding width of 56 nm and 50 nm for 10 µJ and 800 µJ, respectively. These distributions show that for both energies the size distribution is broad compared to chemically synthesized particles.

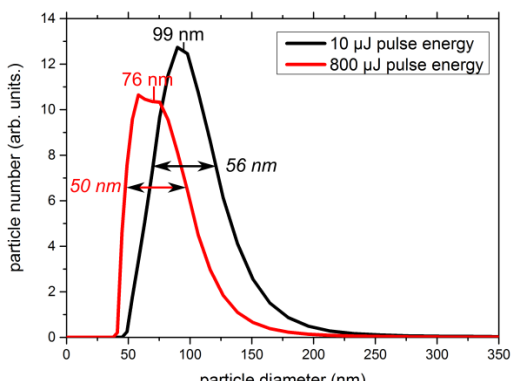

Figure 3: Size distribution of hydrodynamic nanoparticle diameter generated at different pulses energies for optimal ablation conditions at 800 µJ and 10 µJ.

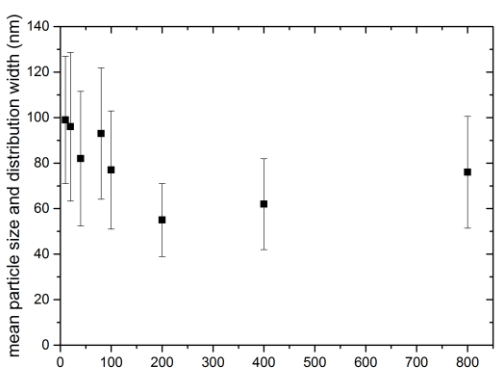

Figure 4: Mean particle size and distribution width of a lognormal fit to the obtained hydrodynamic size distributions generated at different pulse energies.

The dependency of the size distribution on applied pulse energy at optimal efficiency conditions is shown in Figure 4. With increasing pulse energy, the mean particle size decreases from 99 nm at 10 µJ to 56 nm at 200 µJ. For 400 µJ and 800 µJ, the average particle size slightly increases again up to 76 nm. The distribution width is broad (> 40 nm) for all investigated energies.

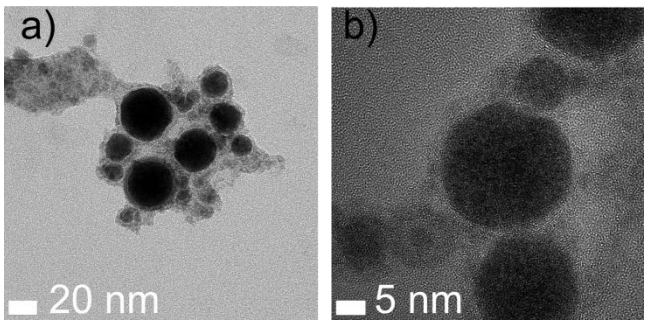

Figure 5: Nanoparticles generated in acetone at a) 800 µJ and b) 10 µJ.

The reason for the different trends in the size distributions is not clear yet. The data shows that it is possible to considerably change the particle size distribution but the dependency and possible mechanisms to control the particle size distribution need to be further investigated. Additionally, it has to be mentioned, that the measurements are averaged over 6 single measurements with an estimated error of 10 % regarding the mean particle size, due to the broad particle size distribution which reduces the reliability of quantitative data.

Figure 5 shows transmission electron microscopy (TEM) images of particles generated in acetone at 800 µJ (a) and 10 µJ (b). The particles generated at both energies show mainly the same composition. The shell consists of amorphous carbon while the core is probably amorphous iron. We could not totally exclude the possibility of an amorphous iron-carbide core meanwhile STEM-EDX (see appendix) measurements suggest that the core consists of amorphous iron.

Further, a small amount of iron-oxide particles was found on the investigated samples.

It was shown that the nanoparticle size distribution can be affected by the pulse energy while the particle composition remains equal. These particles are mostly made of an amorphous iron core with an amorphous carbon shell. The amorphous nature of the particles indicates that in acetone a fast cooling process occurs.

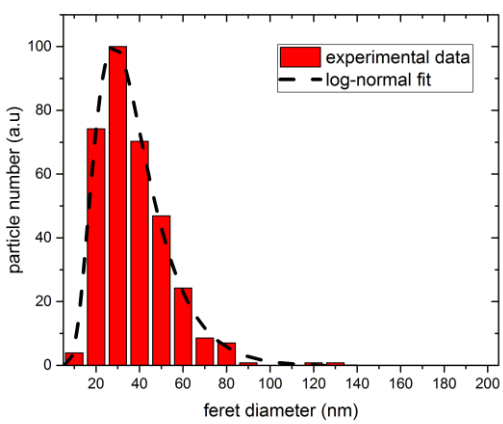

Figure 6: Feret diameter size distribution obtained from TEM pictures for a pulse energy of 800 µJ in water.

3.3. Nanoparticle size distribution and particle composition in water for different laser parameters

In this chapter, the particle size distribution and composition of nanoparticles generated by fs-PLAL in water is presented. In contrast to acetone, water does not possess any organic content. It should be noted that the produced nanoparticles are not stable in water because the isoelectric point is reached at a pH-value between 6 and 7. Thus, the particle size distribution could not be investigated by DLS but was determined by TEM images. Particle size distributions measured by TEM images exhibit slightly lower values than DLS measurements [26].

Similar to the investigation in acetone, the particles have been generated at 800 µJ

pulse energy with optimal bypassing at optimal ablation efficiency conditions.

Figure 6 shows the corresponding feret diameter distribution. The maximum of the particle size distribution was found at 34 nm with a corresponding width of 50 nm.

With regard to the particle composition, Figure 7 shows an exemplary TEM image of the nanoparticles with the corresponding SAED pattern. The particle composition is polycrystalline containing Fe and FeO for the selected areas. This composition is reflected within the TEM images by darker regions showing iron grains while regions with higher transparency belong to FeO. The detailed information about the measured planes is listed in Table 1.

Table 1 SAED patterns of nanoparticles generated in water by iron at 800 µJ and 8,5 µJ pulse energy

d/nm	Fe-Plane	FeO-Plane
0.268	-	(1 1 1)
0.212	(1 1 0)	(2 0 0)
0.149	(2 0 0)	(2 2 0)
0.129	-	(3 1 1)
0.116	(1 1 2)	-
0.104	(2 2 0)	(4 0 0)

Comparing fs-PLAL with literature ns-PLAL results in water, no significant variations can be found. Similar to fs-PLAL, the particles seem to mostly consist of FeO and Fe [12, 17, 18]. In contrast to water, the particle composition in acetone changes from ns-PLAL to fs-PLAL. While ns-PLAL yields more crystalline structures, e.g. developing carbides and oxides, fs-PLAL generated particles are to a large amount amorphous. One reason might be the different heating mechanism of the plasma, yielding a different plasma composition and cooling rate of the plasma plume.

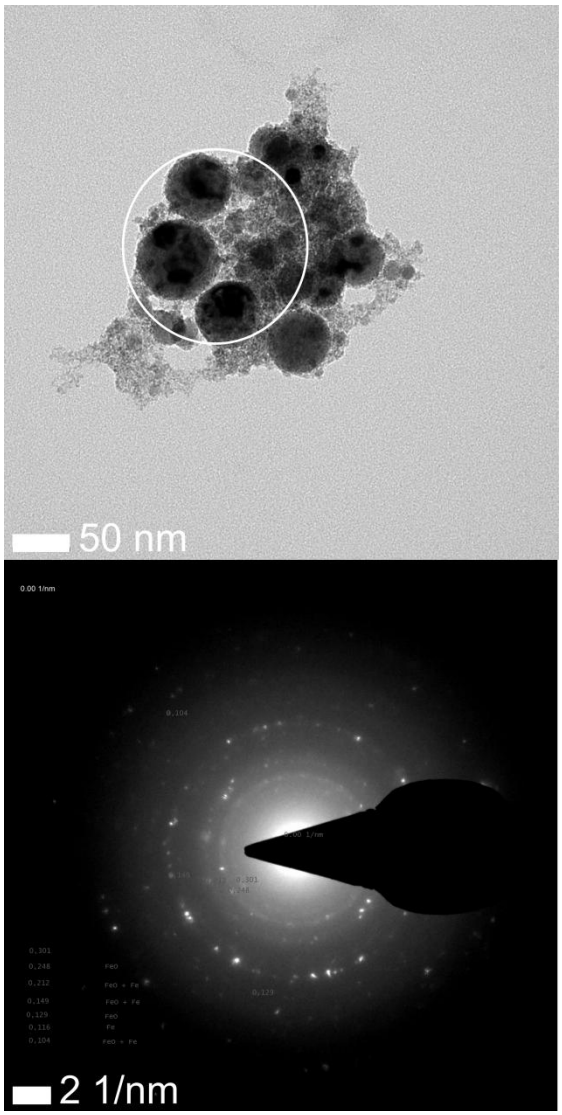

Figure 7: Nanoparticles generated in water (upper image) with the obtained SAED pattern (lower image).

4. Conclusion

This research showed that the particle composition for nanoparticles generated by laser ablation in liquids in the femtosecond range is persevered for different pulse energies. This enables to further investigate the dependency of the particle size distribution on the pulse energy for size distribution tailoring.

Compared to organic liquids, the particle composition does not change when using water as liquid while applying different pulse durations. In order to understand the underlying processes, these differences need to be further investigated.

Acknowledgments
We gratefully acknowledge the financial funding of the DFG within the Project GU1075/3. Furthermore, we would like to thank Dr. Christoph Somsen for the transmission electron microscopy images.

References

1. S. Chikazumi, S. Taketomi, M. Ukita, M. Mizukami, H. Miyajima, M. Setogawa, Y. Kurihara, Journal of Magnetism and Magnetic Materials **65**, 245 (1987)
2. A.-H. Lu, W. Schmidt, N. Matoussevitch, H. Bönnemann, B. Spliethoff, B. Tesche, E. Bill, W. Kiefer, F. Schüth, Angew. Chem. **116**, 4403 (2004)
3. A.K. Gupta, M. Gupta, Biomaterials **26**, 3995 (2005)
4. S. Mornet, S. Vasseur, F. Grasset, P. Veverka, G. Goglio, A. Demourgues, J. Portier, E. Pollert, E. Duguet, Progress in Solid State Chemistry **34**, 237 (2006)
5. T. Hyeon, Chem. Commun., 927 (2003)
6. D.W. Elliott, W.-x. Zhang, Environ. Sci. Technol. **35**, 4922 (2001)
7. J. Köhler, R. Ghadiri, S.I. Ksouri, Q. Guo, E.L. Gurevich, A. Ostendorf, J. Phys. D: Appl. Phys. **47**, 505501 (2014)
8. H. Xia, J. Wang, Y. Tian, Q.-D. Chen, X.-B. Du, Y.-L. Zhang, Y. He, H.-B. Sun, Advanced materials (Deerfield Beach, Fla.) **22**, 3204 (2010)
9. S. Barcikowski, A. Menéndez-Manjón, B. Chichkov, M. Brikas, G. Račiukaitis, Appl. Phys. Lett. **91**, 83113 (2007)
10. H. Zeng, X.-W. Du, S.C. Singh, S.A. Kulinich, S. Yang, J. He, W. Cai, Adv. Funct. Mater. **22**, 1333 (2012)
11. P. Wagener, A. Schwenke, S. Barcikowski, Langmuir : the ACS journal of surfaces and colloids **28**, 6132 (2012)
12. V. Amendola, M. Meneghetti, G. Granozzi, S. Agnoli, S. Polizzi, P. Riello, A. Boscaini, C. Anselmi, G. Fracasso, M. Colombatti, C. Innocenti, D. Gatteschi, C. Sangregorio, J. Mater. Chem. **21**, 3803 (2011)
13. V. Amendola, P. Riello, M. Meneghetti, J. Phys. Chem. C **115**, 5140 (2011)
14. L. Franzel, M.F. Bertino, Z.J. Huba, E.E. Carpenter, Applied Surface Science **261**, 332 (2012)
15. M.B. Agranat, S.I. Anisimov, S.I. Ashitkov, V.V. Zhakhovskii, N.A. Inogamov, K. Nishihara, Y. Petrov, V.E. Fortov, V.A. Khokhlov, Applied Surface Science **253**, 6276 (2007)
16. T. Iwamoto, T. Ishigaki, J. Phys.: Conf. Ser. **441**, 12034 (2013)
17. P. Maneeratanasarn, T. van Khai, S.Y. Kim, B.G. Choi, K.B. Shim, Phys. Status Solidi A **210**, 563 (2013)
18. I.A. Sukhov, A.V. Simakin, G.A. Shafeev, G. Viau, C. Garcia, Quantum Electron. **42**, 453 (2012)
19. B. Neuenschwander, B. Jaeggi, M. Schmid, V. Rouffiange, P.-E. Martin, in *SPIE LASE*, ed. by G. Hennig, X. Xu, B. Gu, Y. Nakata (SPIE, 2012), p. 824307
20. R. Intartaglia, K. Bagga, F. Brandi, Optics express **22**, 3117 (2014)
21. P. Wagener, A. Schwenke, B.N. Chichkov, S. Barcikowski, J. Phys. Chem. C **114**, 7618 (2010)
22. Y. Jee, M.F. Becker, R.M. Walser, J. Opt. Soc. Am. B **5**, 648 (1988)
23. H. Kurita, A. Takami, S. Koda, Appl. Phys. Lett. **72**, 789 (1998)
24. S. Besner, A.V. Kabashin, M. Meunier, Appl. Phys. Lett. **89**, 233122 (2006)
25. R. Intartaglia, K. Bagga, F. Brandi, Optics express **22**, 3117 (2014)
26. C.M. Hoo, N. Starostin, P. West, M.L. Mecartney, J Nanopart Res **10**, 89 (2008)